Quantum Chemical Calculations to Determine Partitioning Coefficients for $HgCl_2$ on Iron-Oxide Aerosols

Sean A. Tacey[†], *Lang Xu*[†], *Tibor Szilvási*[†], *James J. Schauer*[†,‡], *Manos Mavrikakis*[†]*

[†]Department of Chemical and Biological Engineering, 1415 Engineering Drive, University of Wisconsin−Madison, Madison, WI 53706, USA

[‡]Department of Civil and Environmental Engineering, 1415 Engineering Drive, University of Wisconsin−Madison, Madison, WI 53706, USA

Abstract

Gas-to-particle phase partitioning controls the pathways for oxidized mercury deposition from the atmosphere to the Earth's surface. The propensity of oxidized mercury species to transition between these two phases is described by the partitioning coefficient (K_p). Experimental measurements of K_p values for $HgCl_2$ in the presence of atmospheric aerosols are difficult and time-consuming. Quantum chemical calculations, therefore, offer a promising opportunity to efficiently estimate partitioning coefficients for $HgCl_2$ on relevant aerosols. In this study, density functional theory (DFT) calculations are used to predict K_p values for $HgCl_2$ on relevant iron-oxide surfaces. The model is first verified using a NaCl(100) surface, showing good agreement between the calculated (2.8) and experimental (29-43) dimensionless partitioning coefficients at room temperature. Then, the methodology is applied to six atmospherically relevant terminations of α-Fe_2O_3(0001): OH-Fe-R, $(OH)_3$-Fe-R, $(OH)_3$-R, O-Fe-R, Fe-O_3-R, and O_3-R (where R denotes bulk ordering). The OH-Fe-R termination is predicted to be the most stable under typical atmospheric conditions, and on this surface termination, a dimensionless $HgCl_2$ K_p value of 5.2×10^3 at 295 K indicates a strong preference for the particle phase. This work demonstrates DFT as a promising approach to obtain partitioning coefficients, which can lead to improved models for the transport of mercury, as well as for other atmospheric pollutant species, through and between the anthroposphere and troposphere.

Keywords

Density functional theory; Gas-to-particle phase partitioning; Ab-initio phase diagram;
Predictive tool; Adsorption; Gibbs free energy

1. Introduction

The transport of mercury through the atmosphere is of notable concern due to the bioaccumulation of toxic mercury species in aquatic organisms after deposition to the Earth's surface. It is well established that gas-to-particle phase partitioning influences the fate and transport of oxidized mercury (Hg(II)) species in the atmosphere (Amos et al., 2012; Rutter and Schauer, 2007a, 2007b). While both the gas- and particle-phase Hg(II) species deposit readily from the atmosphere, the deposition mechanism (wet or dry) changes depending on the phase. Therefore, it is important to understand the propensity of Hg(II) species to either remain in the gas phase or partition to the particle phase through interactions with aerosols.

Because oxidized gaseous mercury (e.g., $HgCl_2$) is a common chemical form of mercury in both the atmosphere and anthropogenic emissions plumes (Fry et al., 2007; Jew et al., 2015; Jung et al., 2015; Lyman et al., 2016; Niksa and Fujiwara, 2005; Sliger et al., 2000; Tong et al., 2014, 2013; Wilcox, 2009), previous experimental studies have been performed to investigate the partitioning of $HgCl_2$ on a range of aerosols including adipic acid, ammonium sulfate, and sodium chloride (Rutter and Schauer, 2007a, 2007b). The results of these studies showed good agreement with the empirical models for atmospheric mercury transport based on field measurements in the U.S. (Amos et al., 2012). Yet, in order to develop more accurate models for atmospheric mercury transport and deposition, there is still a need to increase the range of aerosols studied, especially those involved in key atmospheric events. For example, dust storms introduce large quantities of dust aerosols that contain notable concentrations of iron oxides (Alghamdi et al., 2015; Chinnam et al., 2006; Mishra et al., 2008; Mori et al., 2003). Also, sea spray releases notable concentrations of sea salt aerosols (predominantly sodium chloride) to the atmosphere (Gong et al., 1997). Past experimental and theoretical studies have shown that iron-oxide and sodium chloride aerosols can potentially influence the phase of Hg(II) species (Rutter and Schauer, 2007b) as well as catalyze their reduction and re-oxidation (Tacey et al., 2016; Tong et al., 2014, 2013). As a result, iron-oxide and sodium chloride aerosols can have significant impacts on the global transport of oxidized mercury through the atmosphere. Moreover, current technologies for mercury capture are based on mercury adsorption (Jain et al., 2010; Wilcox et al., 2012). For example, precious metals (e.g., Pd and Pt) are used in high-temperature coal-gasification processes to preferentially scrub mercury from fuel gas streams. As a result, the target materials should strongly adsorb mercury (i.e., high preference for the particle phase) relative to other common species in Hg-containing streams, e.g., coal-fired power plant effluents (Jain et al., 2010). Thus, the partitioning between the gas and particle phases is a key metric for efficient mercury control technology design.

The fraction of oxidized mercury that partitions to the particle phase can be quantitatively described by the partitioning coefficient, which is related to the following equilibrium reaction:

$$\mathrm{Hg(II)X_2(g) + PM \rightleftharpoons Hg(II)X_2(p)}$$

where PM is the particulate matter, $Hg(II)X_2$ represents the oxidized mercury species (e.g., $HgCl_2$ or $HgBr_2$), and (g) and (p) represent the gas and particle phases, respectively (Amos et al., 2012; Rutter and Schauer, 2007a, 2007b). There are many definitions for the partitioning coefficient, but this study focuses on K_p and $K_\mathrm{p,PM}$, with

$$K_\mathrm{p} = [\mathrm{Hg(II)X_2(p)}]/[\mathrm{Hg(II)X_2(g)}] = [\mathrm{PM}] * K_\mathrm{p,PM} \qquad (1)$$

(square bracket denotes mass concentration). $K_\mathrm{p,PM}$ is K_p weighted by the inverse of the particulate matter concentration ($[\mathrm{PM}]^{-1}$); K_p is dimensionless and $K_\mathrm{p,PM}$ has units of inverse concentration (typically $m^3/\mu g$). While K_p values are calculated in this work, it is important to remember that $K_\mathrm{p,PM}$ is commonly used in experimental work for determining Hg(II) partitioning coefficients. However, the experimental process to obtain accurate partitioning coefficients in the presence of aerosols, such as dust (iron-oxide), is time-consuming.

Here, an alternative method is proposed based on quantum chemical calculations. Gas-to-particle phase partitioning involves the adsorption of molecules on surfaces, which can be modeled by using state-of-the-art electronic-structure methods. Density functional theory (DFT) (Burke and Wagner, 2013; Dreizler and Gross, 1990; Engel and Dreizler, 2011; Koch and Holthausen, 2001; Parr and Yang, 1984; Sholl and Steckel, 2009) has been successfully used to model surface-adsorbate interactions, either by itself as a predictive tool (Nørskov et al., 2004; Xu et al., 2016) or in comparisons (typically in close agreement) with experimental results (Gautier et al., 2015), for a variety of physical and chemical processes including species adsorption on aerosol surfaces (Tacey et al., 2016). Here, the partitioning coefficient of $HgCl_2$ is calculated in the presence of aerosols using DFT, which can be a relatively fast, albeit reasonably accurate, alternative to time-consuming and complicated experimental measurements.

In particular, the goal of this study is to calculate the partitioning coefficient of $HgCl_2$ on a range of extended aerosol surfaces. First, the appropriateness of the computational approach is detailed by benchmarking the calculated partitioning coefficient results against previously determined experimental values. For this purpose, results are used for NaCl aerosols, on which well-established partitioning coefficients are available in the experimental literature (Rutter and Schauer, 2007b). Then, the thermodynamically most stable iron-oxide surfaces are modeled to calculate the $HgCl_2$ partitioning coefficient on a few selected surfaces. The gas-particle partitioning of reactive mercury in the atmosphere plays a critical role in the fate and transport of mercury (Amos et al., 2012) and has important implications for measurement approaches (Rutter et al., 2008a, 2008b). Although partitioning estimates of reactive Hg in the atmosphere are important to understanding sampling artifacts, designing reactive mercury measurement methods, and modeling the fate of mercury, there are only a limited number of tools to obtain such estimates. The subject work addresses the need for a theoretical basis to quantify reactive mercury partitioning and demonstrates the ability of such computational tools to support atmospheric mercury studies. This model can also be utilized to implement a high-throughput methodology for obtaining information on partitioning coefficients for other environmental pollutants on a range of aerosols.

2. Methods

To determine energetic and geometric parameters, as well as vibrational frequencies, for gas-phase and adsorbed $HgCl_2$, plane-wave DFT calculations were performed through the Vienna

Ab-initio Simulation Package (VASP) (Kresse and Furthmüller, 1996a, 1996b). A detailed description of the calculation setup can be found in Supporting Information. To design a computationally efficient approach, a slab model involving homogeneous aerosol surfaces without impurities present is used, and adsorption is limited to one side of the slab. Similar slab models have been commonly used in DFT studies for heterogeneous catalytic systems (Liu et al., 2017; Xu et al., 2018). While this model is a simplification of the actual aerosol particles, it is later shown that the agreement between the calculated and experimental results is within 5 kJ/mol. A more complicated model will not significantly improve the model accuracy to necessitate the associated increase in computational cost.

The validity of the model was tested by studying $HgCl_2$ adsorption on NaCl aerosols using a NaCl(100) slab model (Figure 1). In addition, to model $HgCl_2$ adsorption on iron-oxide aerosols, several α-Fe_2O_3(0001) slabs were studied. Depending on the environmental conditions, various α-Fe_2O_3(0001) surface terminations may be present; and for that, 13 different terminations were considered in this study (Figure S1). To determine relevant terminations under typical atmospheric conditions from first principles, phase diagrams were constructed plotting the surface Gibbs free energy (γ) versus parameters that depend on O_2 partial pressure and relative humidity. The detailed procedure for the phase diagram construction is described in Supporting Information.

Two important energetic parameters used throughout this work are the adsorption (binding) energy and Gibbs free energy of adsorption. The adsorption energy (E_B) is defined as

$$E_\mathrm{B} = E_\mathrm{tot} - E_\mathrm{slab} - E_\mathrm{gas} \qquad (2)$$

where E_tot is the total energy of $HgCl_2$ adsorbed on the aerosol surface, E_slab is the energy of the clean aerosol surface, and E_gas is the DFT-calculated energy of gas-phase $HgCl_2$. By this definition, E_B is evaluated using electronic energies obtained by DFT at 0 K. When dealing with atmospheric chemistry, it is important to use thermodynamic quantities that can be evaluated over a range of temperatures and pressures. Therefore, the Gibbs free energy of adsorption (G_B) is defined as

$$G_{\mathrm{B}} = (h - Ts)_{\mathrm{ads}} - E_{\mathrm{slab}} - (h - Ts)_{\mathrm{gas}} \tag{3}$$

where T is the temperature, h is the molar enthalpy, s is the molar entropy, and the "ads" and "gas" subscripts refer to systems with adsorbed and gas-phase $HgCl_2$, respectively. Both E_B and G_B reflect the strength of the interaction between $HgCl_2$ and the modeled surface; the more negative the value the stronger the interaction.

The focus of the adsorption studies was placed on the high-symmetry sites of each surface (Figure 1). Various initial orientations of $HgCl_2$ above each surface were studied to ensure that adsorption structures corresponding to the global minimum (i.e., the structure with lowest G_B value) and to various local minima on the potential energy surface were located. These calculations were performed at low, fixed $HgCl_2$ coverages (one $HgCl_2$ species per unit cell, which corresponds to 1/4 and 1/16 monolayer for the (2 × 2) α-Fe_2O_3(0001) and (4 × 4) NaCl(100) surface unit cells, respectively). Further increasing the unit cell size (i.e., lowering the $HgCl_2$ surface coverage) leads to changes of <3 kJ/mol in calculated binding energies. Therefore, the calculated binding properties are close estimates of those at the low-coverage limit. Because the concentration of atmospheric $HgCl_2$ is much lower compared to the number of available aerosol surface sites (~1:10^3) (Tong et al., 2014), the current unit cell setup is a reasonable model of real aerosol surfaces in the troposphere.

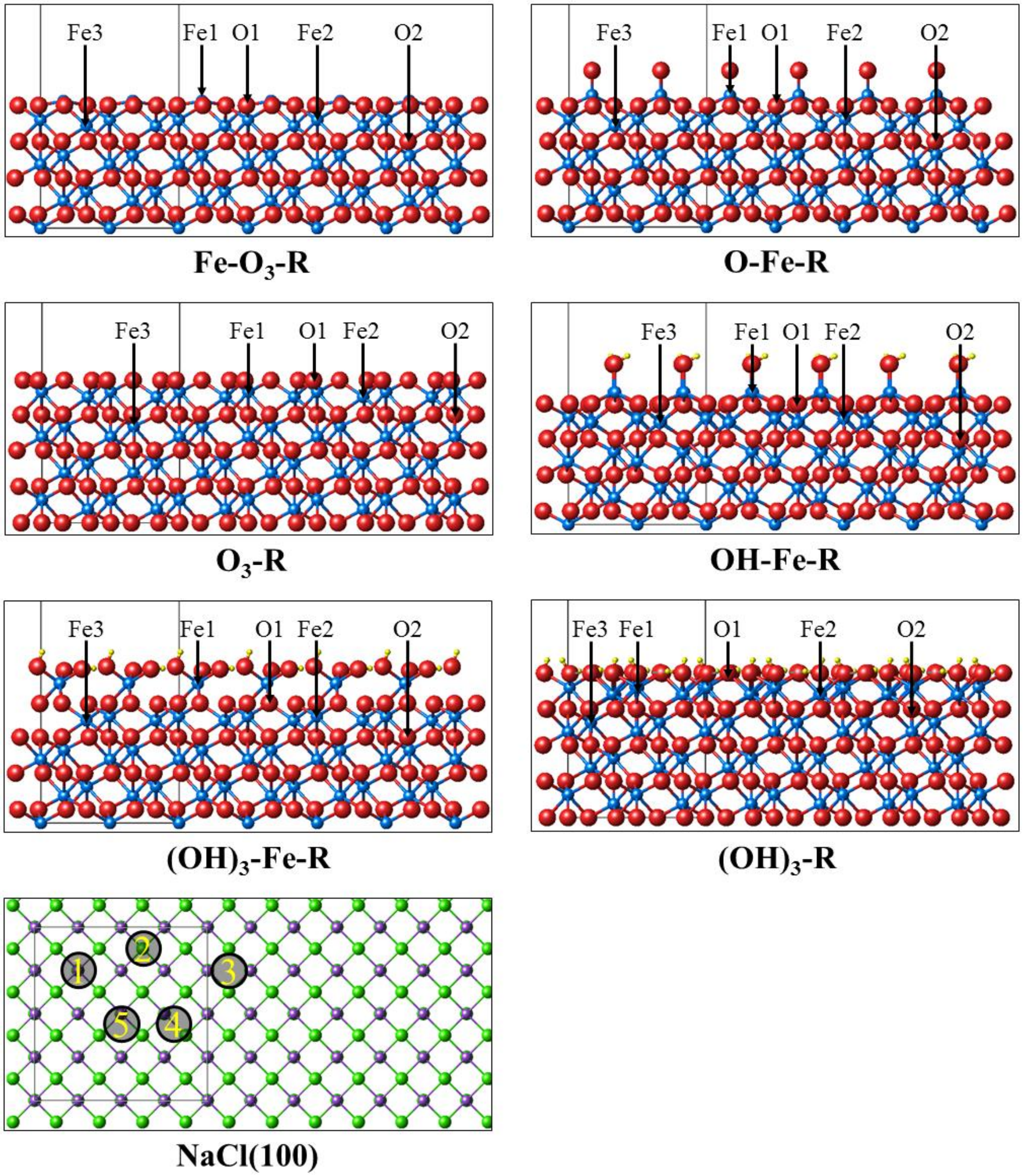

Figure 1. High-symmetry sites for each studied surface. For the α-Fe_2O_3(0001) surfaces the sites are indicated by arrows, using the notation Xy, where X is a specific atom and y is the atom's corresponding layer number (e.g., Fe1 indicates that $HgCl_2$ is placed over an iron atom in the first iron layer). For NaCl(100), the high-symmetry sites (depicted by a top view of the slab) are: 1 – top(Na); 2 – top(Cl); 3 – bridge(Na-Na); 4 – bridge(Na-Cl); and 5 – threefold hollow. Atom colors are given by: blue – Fe; red – O; yellow – H; green – Cl; and purple – Na. Solid black lines indicate the unit cell.

To determine the partitioning coefficient of $HgCl_2$ on atmospherically relevant aerosol surfaces, the following definition of dimensionless K_p was used according to the Boltzmann distribution

$$K_\mathrm{p} = [\mathrm{PM}]K_\mathrm{p,PM} = \frac{\sum_j K_{\mathrm{p},j} \exp\left(-\left(G_{\mathrm{B},j} - G_\mathrm{B,min}\right)/k_\mathrm{B}T\right)}{\sum_j \exp\left(-\left(G_{\mathrm{B},j} - G_\mathrm{B,min}\right)/k_\mathrm{B}T\right)} \quad (4)$$

where j corresponds to individual adsorption structures of $HgCl_2$ on the aerosol surface, k_B is the Boltzmann constant, and $K_{p,j}$ is the partitioning coefficient for adsorption structure j, given by

$$K_{\mathrm{p},j} = \exp\left(-G_{\mathrm{B},j}/k_\mathrm{B}T\right) \quad (5)$$

Note that the dimensionless partitioning coefficients, as shown by Equation (4), can be expressed without including the particulate matter concentration ([PM]). Because aerosol concentrations exhibit spatial and temporal variations in the atmosphere, the approach allows for easy implementation of the calculated partitioning coefficient values in atmospheric mercury transport models as long as the aerosol type is known or can be estimated based on thermodynamics.

3. Results and Discussion

In this section, the results are presented in the following order. First, the proposed DFT-based method is validated by calculating partitioning coefficients for $HgCl_2$ in the presence of NaCl, as experimental results are available for this system. Second, *ab-initio* phase diagrams are constructed to determine relevant α-Fe_2O_3(0001) surface terminations under tropospheric conditions. Third, adsorption energetics and structures are determined for $HgCl_2$ on tropospherically relevant α-Fe_2O_3(0001) surfaces. Lastly, these adsorption parameters are applied to the DFT-based method to calculate dimensionless partitioning coefficients for $HgCl_2$ on the considered iron-oxide surfaces.

3.1. Method Validation

Here, the proposed DFT-based method to determine partitioning coefficients for $HgCl_2$ in the presence of aerosol surfaces is validated by calculating the Gibbs free energy of adsorption of $HgCl_2$ on the NaCl(100) surface. Because experimental partitioning coefficients for $HgCl_2$ in the presence of NaCl aerosols have been previously reported in the literature (Rutter and Schauer, 2007b), NaCl(100) can be used as a test case to validate the approach.

The adsorption search provided three stable $HgCl_2$ adsorption structures on the NaCl(100) surface with E_B values within 20 kJ/mol of the minimum-energy structure. A summary of adsorption structures is listed in Tables S1 and S2. The most stable adsorption structure for $HgCl_2$ on NaCl(100) shows an E_B value of –65 kJ/mol and a G_B value of –4 kJ/mol at 295 K (Figure 2). Assuming a Boltzmann distribution at room temperature, it is important to stress that a difference in G_B of roughly 6 kJ/mol between two adsorption structures corresponds to an order-of-magnitude difference in the abundance of $HgCl_2$ in those specific adsorption structures. Therefore, adsorption structures with lower (i.e., more negative) Gibbs free energies of adsorption have notably more weight (see exponential weight factor in Equation 4) than those showing higher values when calculating the partitioning coefficient. Indeed, adsorption structures more than 20 kJ/mol less stable than the global minimum have negligible contributions to the partitioning coefficient, as the Boltzmann distribution predicts extremely small weights ($<10^{-4}$) at temperatures relevant for tropospheric processes (250 K to 315 K). Thus, only the three adsorption structures found within 20 kJ/mol of the identified global minimum were used for calculating the overall partitioning coefficient. The energetic parameters for these structures are noted in Table S1 and S2.

Using the G_B values obtained in a temperature range between 250 and 315 K, the partitioning coefficient for $HgCl_2$ was calculated in the presence of the NaCl(100) aerosol surface. The calculated K_p values are 1.2×10^2, 2.8×10^0, and 7.6×10^{-1} at 250 K, 295 K, and 315 K, respectively. Rutter and co-workers reported an experimental $K_{p,PM}$ range of 20–30 $m^3/\mu g$ (with a standard deviation of 8.5 $m^3/\mu g$) at 290–295 K and a total NaCl aerosol mass concentration of 1.44 $\mu g/m^3$ (2007b). Therefore, their experimental, dimensionless K_p values range from 29 to 43 at 290–295 K. As such, predicted $HgCl_2$ partitioning coefficients agree well (within an order of magnitude) with those determined experimentally for NaCl aerosols.

While a good general agreement between the proposed model and experiments is achieved, there are potential reasons for the observed differences. First, for calculations considering similar systems, DFT errors are largely systematic. The experimental partitioning coefficient range corresponds to an average G_B value of –9 kJ/mol, while the calculations performed here suggest an average G_B value of –4 kJ/mol. The 5 kJ/mol difference is well within the systematic error in DFT of 10-20 kJ/mol (Sholl and Steckel, 2009). Similar differences can be expected for the iron-oxide surfaces, allowing for reasonable comparison of the $HgCl_2$ K_P values. Second, harmonic approximations were made in the entropy calculations. It has been shown for long-chain hydrocarbons that harmonic approximations can potentially underestimate adsorption entropies (Campbell and Sellers, 2012); however, because the size and adsorption properties of $HgCl_2$ are different, the correction terms derived for hydrocarbons to account for anharmonicity were not used. While these factors can influence the partitioning coefficient calculation, the results shown here demonstrate that DFT calculations are a viable approach for the prediction of partitioning coefficients.

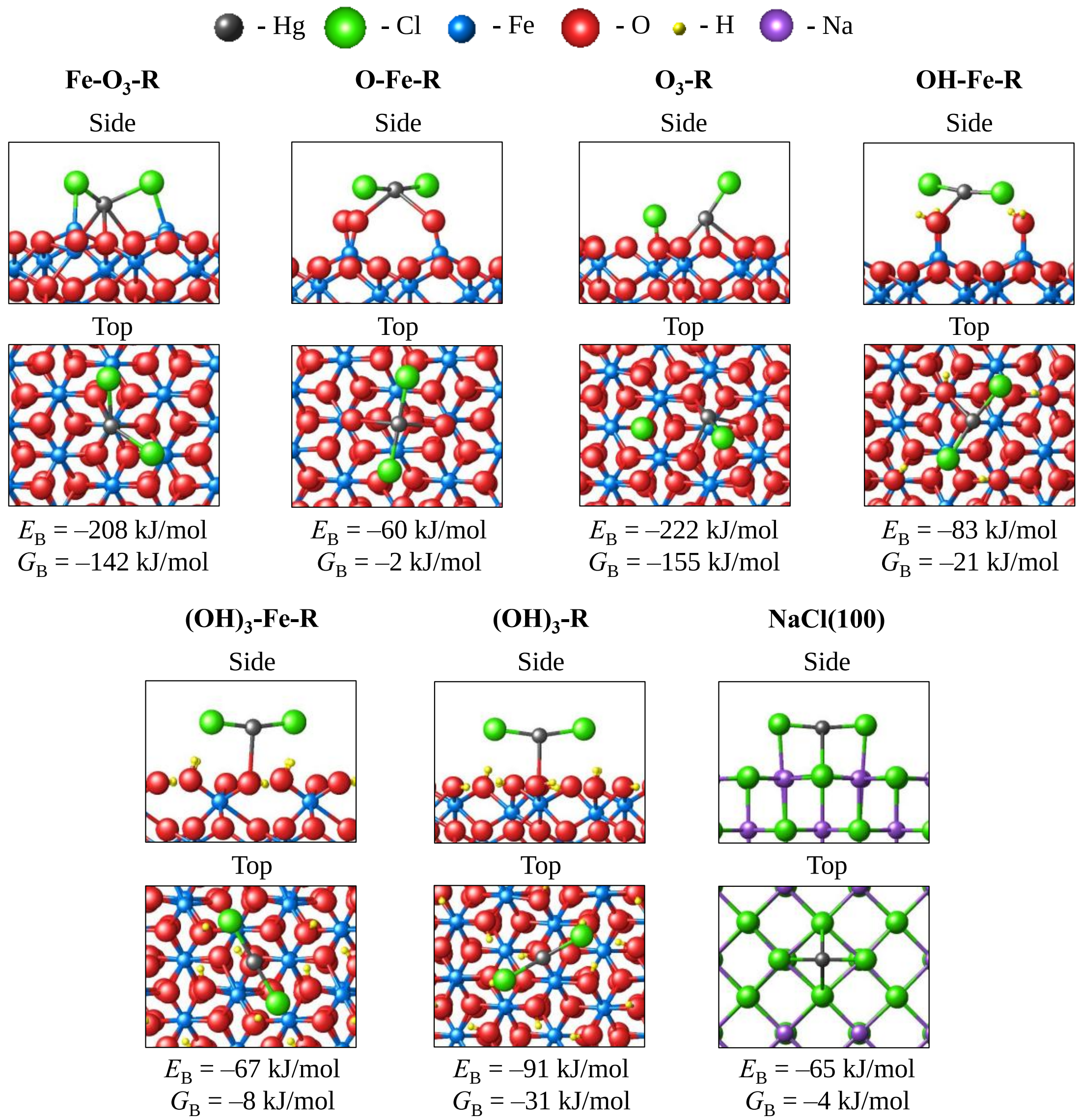

Figure 2. Cross-sectional (side) and top views of the optimal $HgCl_2$ adsorption structures on each of the studied surfaces. Energies and Gibbs free energies of adsorption (E_B and G_B, respectively) are provided for each structure, with G_B values provided at 295 K.

3.2. Determining Relevant Iron-Oxide Surface Terminations

In this section, DFT is used to construct phase diagrams for the α-Fe_2O_3(0001) surface, which account for the interactions of atmospheric water and oxygen with the α-Fe_2O_3(0001) surface. The phase diagram allows one to determine which surface termination has the lowest surface Gibbs free energy (i.e., thermodynamically most stable) at various conditions. This approach has also been described as the *ab-initio* thermodynamics method in the past literature (Aboud et al., 2011; Negreira et al., 2011). Using this information, the terminations of the α-Fe_2O_3(0001) surface that are the most relevant under atmospheric conditions are determined.

Before calculating the partitioning coefficient of $HgCl_2$ on iron-oxide aerosols, the relevant surface terminations of α-Fe_2O_3(0001) were determined under atmospheric conditions. A range of surfaces under varying coverages of O, OH, and H_2O were evaluated to simulate the effects of oxygen and water in the atmosphere (Figure S1), as it is well established in the literature that the presence of oxygen and water can influence the surface of metal oxides (Aboud et al., 2011; Barbier et al., 2007; Negreira et al., 2011). Thermodynamics calculations were performed to determine the optimal arrangement of O, OH, and H_2O on the iron-oxide surface at each level of coverage. Further, the relative stability of each surface termination was determined by constructing *ab-initio* phase diagrams. Comparisons with experimental work suggest that DFT calculations better predict the relevant surface terminations as compared to those predicted by DFT+*U* calculations (Barbier et al., 2007); therefore, to compare the quality of the two methods in this specific case, *ab-initio* phase diagrams were created with both DFT and DFT+*U* (Figures 3 and S2, respectively). The white lines in each phase diagram represent the atmospherically relevant ranges for the H_2O and O_2 chemical potentials. These ranges capture a fixed oxygen partial pressure of 0.21 bar, a range of temperatures between –20 °C and 40 °C, and a range of relative humidity from 0.01 to 1. By incorporating relative humidity and oxygen partial pressure, the interactions of water and oxygen with the α-Fe_2O_3(0001) surface were considered. These interactions are important for the accurate representation of the α-Fe_2O_3(0001) surface in the atmosphere.

Under the studied conditions, both DFT methods predict that the OH-Fe-R termination is the most stable (Region A in both Figures 3 and S2), where R denotes the bulk ordering. However, due to the generally considered 10-20 kJ/mol error of DFT, the results from the two phase diagrams using the Perdew-Burke-Ernzerhof functional with density dependent dispersion corrections (PBE-dDsC and PBE-dDsC+U; more details in the SI) indicate that the $(OH)_3$-Fe-R and $(OH)_3$-R terminations, respectively, may also be stable (yellow box around region A in Figures 3 and S2). Additionally, under significantly dry conditions ($x_{\mathrm{H_2O}}$~0), the PBE-dDsC phase diagram predicts that the O-Fe-R surface is most stable (Region B in Figure 3), consistent with previous experimental and theoretical findings (Barbier et al., 2007). Also, work on the α-Fe_2O_3(0001) surface in the literature have focused on the Fe-O_3-R and O_3-R terminations (Baltrusaitis et al., 2014; Hellman and Pala, 2011), so the stability regions for these surfaces were also examined. On the PBE-dDsC phase diagram, the Fe-O_3-R and O_3-R terminations would correspond to local oxygen-poor and oxygen-rich environments (Regions C and D in Figure 3 represent sample conditions for these regions). Because of these observations, this study will focus on the following six α-Fe_2O_3(0001) surface terminations in this work: Fe-O_3-R, O-Fe-R, O_3-R, OH-Fe-R, $(OH)_3$-Fe-R, and $(OH)_3$-R (Figure 1).

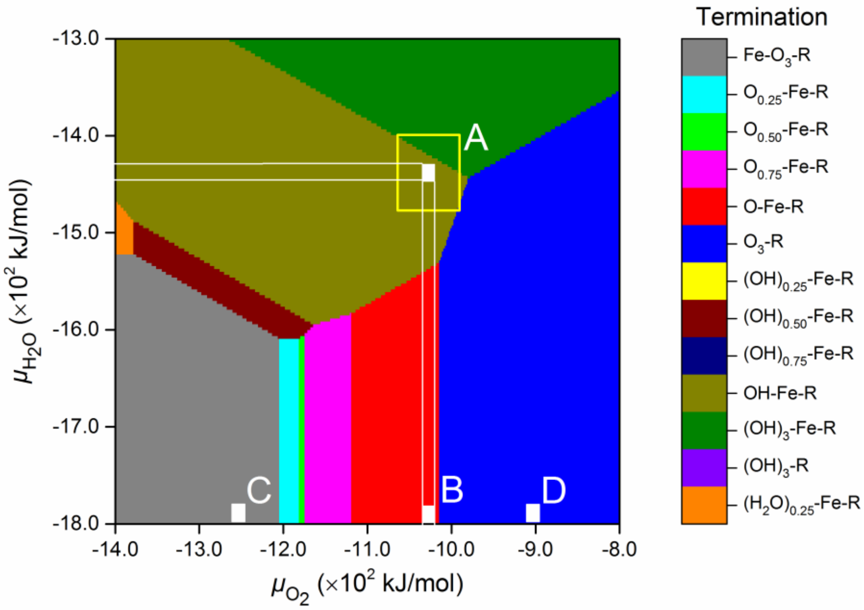

Figure 3. Phase diagram (DFT, PBE-dDsC) for the α-Fe_2O_3(0001) surface as a function of oxygen (μ_{O_2}) and water (μ_{H_2O}) chemical potential. The vertical and horizontal white lines represent the typical range for $\mu_{O_2}$and μ_{H_2O} at a fixed oxygen partial pressure of 0.21 bar, a range of relative humidity from 0.01 to 1, and a temperature range of –20 to 40 °C. Regions A, B, C, and D denote the atmospherically relevant regions for normal, dry, low oxygen, and high oxygen tropospheric conditions, respectively. The yellow box surrounding region A encapsulates the range for DFT error.

3.3. Adsorption of $HgCl_2$ on Iron-Oxide Aerosol Surfaces

With the most representative α-Fe_2O_3(0001) surfaces identified, relevant $HgCl_2$ adsorption descriptors were calculated on these surfaces. Different orientations and positions of $HgCl_2$ above the surfaces were evaluated to determine which adsorption structures are most stable by calculating G_B at tropospherically relevant temperatures between –20 to 40 °C.

After determining the relevant surface terminations of α-Fe_2O_3(0001), the adsorption of $HgCl_2$ on each iron-oxide surface was probed, using a similar $HgCl_2$ Gibbs free energy of adsorption criterion for the iron-oxide surfaces as for the NaCl(100) surface to determine the relevant adsorption structures. The $HgCl_2$ adsorption analyses suggested 5 or 6 unique structures on each surface for calculating the $HgCl_2$ partitioning coefficient. The adsorption structures showing the minimum value of G_B for each surface are shown in Figure 2, while a more comprehensive summary of adsorption structures can be found in Tables S1 and S2.

The O_3-R-terminated α-Fe_2O_3(0001) surface binds $HgCl_2$ dissociatively, leaving HgCl and Cl adsorbed on the surface, with a Gibbs free energy of adsorption of –155 kJ/mol at 295 K. The rest of the studied α-Fe_2O_3(0001) surfaces bind $HgCl_2$ molecularly. On the Fe-O_3-R-terminated α-Fe_2O_3(0001) surface, the calculated G_B value of the optimal adsorption structure is –142 kJ/mol at 295 K. The calculated G_B values indicate a propensity for strong adsorption of $HgCl_2$ on both the O_3-R- and Fe-O_3-R-terminated surfaces.

On the $(OH)_3$-R-terminated α-Fe_2O_3(0001) surface, the optimal $HgCl_2$ adsorption structure has a Gibbs free energy of adsorption of –31 kJ/mol at 295 K. Furthermore, on the OH-Fe-R-terminated α-Fe_2O_3(0001) surface, which is predicted to be the most stable termination of α-Fe_2O_3(0001) by both phase diagrams presented in Section 3.2, $HgCl_2$ adsorbs in the ground-state configuration with a Gibbs free energy of adsorption of –21 kJ/mol at 295 K. $HgCl_2$ does not bind as strongly to these two surfaces as on the Fe-O_3-R- and O_3-R- terminated surfaces. Lastly, $HgCl_2$ binds the weakest on the $(OH)_3$-Fe-R and the O-Fe-R α-Fe_2O_3(0001) surface terminations, with Gibbs free energies of adsorption of –8 and –2 kJ/mol at 295 K, respectively. As a result, $HgCl_2$ desorption is more likely to occur from these two surfaces as compared to the other four surfaces.

The importance of correcting the adsorption energies for temperature effects can be readily assessed from the data provided in Figure 2. DFT calculates energies at 0 K, leading to notable changes in the adsorption energy of around 60-70 kJ/mol after temperature corrections to 295 K are made. Adsorption of $HgCl_2$ onto the aerosol surfaces results in the loss of one translational degree of freedom. Thus, the difference between E_B and G_B values at 295 K are due in large part to entropic effects, where the entropy change upon adsorption at 295 K accounted for 40 to 50 kJ/mol of this difference across the studied surfaces. Because the partitioning coefficient calculation involves an exponential term for the adsorption energy, not accounting for temperature corrections to the energetics would lead to partitioning coefficients that would be, for the temperature range of interest, several orders-of-magnitude (ten to twelve) greater than those with the temperature corrections included.

3.4. $HgCl_2$ Partitioning Coefficients

Lastly, the calculated Gibbs free energies of adsorption were used to calculate the partitioning coefficients of $HgCl_2$ on the selected α-Fe_2O_3(0001) surfaces as a function of temperature. Several relevant $HgCl_2$ adsorption structures for each surface are fit through a Boltzmann distribution to calculate the overall "fitted" partitioning coefficient. The Boltzmann distribution employs a Gibbs free energy of adsorption for each mode, giving more weight to adsorption structures with lower G_B values (see Equation (4)).

Once the adsorption structures for $HgCl_2$ on each aerosol surface were determined, along with the corresponding Gibbs free energies of adsorption, partitioning coefficients were calculated according to Equation (4). A summary of the partitioning coefficient data is shown in Figure 4 as a $\log_{10}(K_p)$ vs. Temperature plot (tabulated data can be found in Table S2). Results for the Fe-O_3-R- and O_3-R-terminated α-Fe_2O_3(0001) surface are not shown in this plot as the Gibbs free energies of adsorption suggest a significantly strong interaction with these clean aerosol surfaces. These results indicate that under the oxygen-rich and oxygen-poor conditions mentioned before, there is a strong tendency for $HgCl_2$ to partition to the particle phase.

On the $(OH)_3$-R and OH-Fe-R (predicted to be the most stable by the phase diagram calculations) α-$Fe_2O_3(0001)$ surface terminations, the partitioning coefficient values range from 6.1×10^7 and 6.1×10^5 at 250 K to 4.0×10^4 and 1.0×10^3 at 315 K, respectively. These values indicate that $HgCl_2$, in the presence of these surface terminations, is predominantly in the particle phase even in the high-temperature limit. On the $(OH)_3$-Fe-R surface termination of α-$Fe_2O_3(0001)$, $HgCl_2$ is predicted to have lower partitioning coefficient values: 6.7×10^2 and 5.7×10^0 at 250 K and 315 K, respectively. However, at both the low- and high-temperature limits, the partitioning coefficient values are above 1, indicating that $HgCl_2$ still prefers the particle phase in the presence of this aerosol surface, yet to a lesser degree compared to the $(OH)_3$-R and OH-Fe-R terminations of the α-$Fe_2O_3(0001)$ surface.

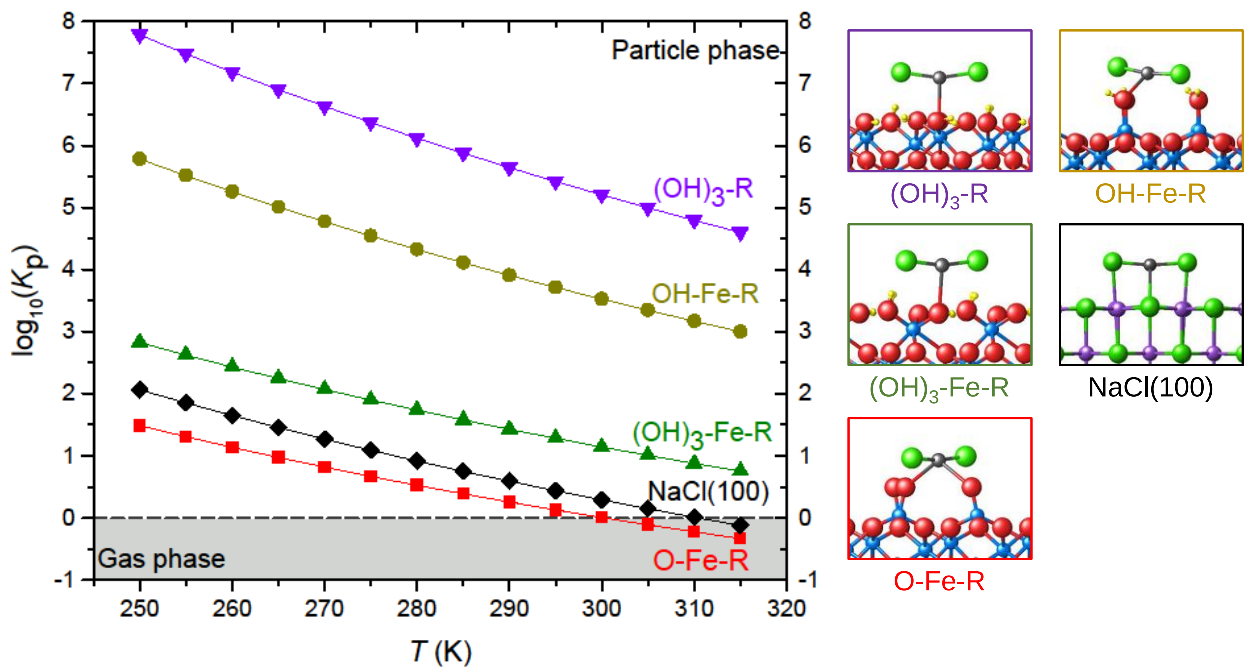

Figure 4. Plot of $\log_{10}(K_p)$ vs. Temperature (K) for the iron-oxide and sodium chloride aerosol surfaces considered in this study. The horizontal dashed line separates regions where the particle (unshaded region) and gas (shaded region) phases are preferred. Results for the Fe-O_3-R and O_3-R terminations are not shown as $HgCl_2$ undergoes irreversible adsorption in the presence of these two surfaces (K_p approaches infinity). For clarity, adsorption structures for each surface in this

plot are provided, and atom colors are: grey – Hg; green – Cl; blue – Fe; red – O; and yellow – H.

The results are notably different for the remaining O-Fe-R α-Fe_2O_3(0001) surface termination. At the low-temperature limit (250 K) the partitioning coefficient was calculated to be 3.1×10^{1}, whereas at the high-temperature limit (315 K) the partitioning coefficient reduces to 4.7×10^{-1}. This finding indicates that $HgCl_2$ is preferentially in the gas phase at temperatures above 300 K, where the dimensionless partitioning coefficient equals 1 (see Equation 1).

Due to the definition of K_p adopted for this study (Equation (4)), there exists a linear dependence of $\log_{10}(K_p)$ on the Gibbs free energy of adsorption (Figure S3), which is consistent with the previous experimental studies on calculating mercury partitioning coefficients (Rutter and Schauer, 2007a). Moreover, the predicted partitioning coefficients for $HgCl_2$ in the presence of iron-oxide aerosols show high variability depending on the α-Fe_2O_3(0001) surface termination that is present (i.e., the surrounding atmospheric conditions). This variability is significant as the partitioning coefficient ranges from below 1 (gas phase preferred) to well above 1 (particle phase preferred) in a temperature range of 250 to 315 K. The wide range of partitioning coefficients can largely influence the transport and deposition processes that $HgCl_2$ undergoes in the presence of iron-oxide aerosols in the atmosphere. Thus, if one were to study the partitioning coefficient for $HgCl_2$ on iron-oxide aerosols, either experimentally or in mercury transport models, significant care should be taken to note the atmospheric conditions, which impacts the exposed iron-oxide surface termination.

In addition, this work focuses solely on the adsorption properties for $HgCl_2$ on the iron-oxide surfaces. Aside from the O_3-R surface where dissociative adsorption occurs, the reaction of $HgCl_2$ (e.g., Hg-Cl bond breaking) on the studied surfaces was not considered. While reactions may occur after $HgCl_2$ adsorption, the partitioning coefficients ultimately dictate the propensity for $HgCl_2$ adsorption. The possible reactions that $HgCl_2$ undergoes on the iron-oxide surface following adsorption will be discussed in a separate paper in the future.

Furthermore, because certain terminations of the iron-oxide surface result in different $HgCl_2$ partitioning coefficients, progress in mercury capture technology design can be made, as metal and metal-oxide sorbents are commonly used for high-temperature capture processes. By showing that the environment (relative humidity, oxygen partial pressure, and temperature) affects the occurrence of specific surface terminations, and therefore the partitioning coefficient, obtaining a realistic picture of the surface under conditions relevant in, e.g., coal-fired power plant effluent streams, becomes extremely important. This knowledge allows for searching for new effective mercury scrubbing strategies. Indeed, an optimal mercury capture material should have a high partitioning coefficient to preferentially scrub mercury to the particle phase. By understanding which surfaces of a metal/metal oxide achieve high mercury partitioning coefficients, one can potentially tune surrounding conditions to maximize mercury partitioning to the particle phase.

4. Conclusions

In this study, quantum chemical calculations based on DFT were shown to efficiently calculate partitioning coefficients for $HgCl_2$ in the presence of a range of iron-oxide and sodium chloride aerosol surfaces with a reasonable degree of accuracy. First, it was shown that the model provides order-of-magnitude agreement for the partitioning coefficient of $HgCl_2$ on a NaCl aerosol surface, with calculated (2.8) and experimental (29-43) dimensionless partitioning coefficient values. Then, the model was extended to calculate the partitioning coefficient on six tropospherically relevant α-Fe_2O_3(0001) surface terminations. The phase diagram analysis showed that the OH-Fe-R surface termination is most relevant, and a dimensionless partitioning coefficient of 5.2×10^3 was calculated on this surface at a temperature of 295 K.

Further, the definition of the partitioning coefficient adopted in this study, expressed as a dimensionless number not adjusted for a specific PM concentration, allows for a more general implementation of the calculated values into, e.g., transport models or controls technology design. The successful implementation of DFT in this study is especially promising, as the techniques and expressions used to calculate the partitioning coefficients can be adapted to calculate other parameters of interest. For example, one could use DFT to efficiently screen the partitioning coefficients for other atmospheric pollutants on a range of aerosols or to obtain energetic/kinetic data used to better model the physical and chemical processes that species undergo in the atmosphere. DFT is widely used in the field of surface science, and as this study shows, can be readily adapted to tackle problems in the field of atmospheric chemistry.

Appendix A. Supplementary data

Supplementary data to this article is available online.

Corresponding Author
*Corresponding author
Email: emavrikakis@wisc.edu
Phone: (608) 262–9053
Fax: (608) 262–9053

Acknowledgements

The authors thank Dr. Florian Göltl and Dr. Roberto Schimmenti for carefully proofreading the manuscript and for providing very useful comments. The work was partly supported by the UW-

Madison graduate school and by the Grainger Wisconsin Distinguished Graduate Fellowship. Additional funds were provided by the Air Force Office of Scientific Research Grant FA9550-16-1-0141. Computational work was performed partly through supercomputing resources from the following institutions: The National Energy Research Scientific Computing Center (NERSC); the Center for Nanoscale Materials (CNM) at Argonne National Laboratory (ANL); and the Environmental Molecular Sciences Laboratory (EMSL), a national scientific user resource located at Pacific Northwest National Laboratory (PNNL). EMSL is supported by the DOE Office of Biological and Environmental Research at PNNL. CNM and NERSC are supported by the U.S. DOE, Office of Science, under Contract Nos. DE-AC02-06CH11357 and DE-AC02-05CH11231, respectively.

References

Aboud, S., Wilcox, J., Brown Jr., G.E., 2011. Density functional theory investigation of the interaction of water with α-Al_2O_3 and α-$Fe_2O_3(1\bar{1}02)$ surfaces: Implications for surface reactivity. Phys. Rev. B 83, 125407–125422. https://doi.org/10.1103/PhysRevB.83.125407

Alghamdi, M.A., Almazroui, M., Shamy, M., Redal, M.A., Alkhalaf, A.K., Hussein, M.A., Khoder, M.I., 2015. Characterization and elemental composition of atmospheric aerosol loads during springtime dust storm in western Saudi Arabia. Aerosol Air Qual. Res. 15, 440–453. https://doi.org/10.4209/aaqr.2014.06.0110

Amos, H.M., Jacob, D.J., Holmes, C.D., Fisher, J.A., Wang, Q., Yantosca, R.M., Corbitt, E.S., Galarneau, E., Rutter, A.P., Gustin, M.S., Steffen, A., Schauer, J.J., Graydon, J.A., St. Louis, V.L., Talbot, R.W., Edgerton, E.S., Zhang, Y., Sunderland, E.M., 2012. Gas-particle partitioning of atmospheric Hg(II) and its effect on global mercury deposition. Atmos.

Chem. Phys. 12, 591–603. https://doi.org/10.5194/acp-12-591-2012

Baltrusaitis, J., Hu, Y.-S., McFarland, E.W., Hellman, A., 2014. Photoelectrochemical hydrogen production on α-Fe_2O_3(0001): Insights from theory and experiments. ChemSusChem 7, 162–171. https://doi.org/10.1002/cssc.201300715

Barbier, A., Stierle, A., Kasper, N., Guittet, M.-J., Jupille, J., 2007. Surface termination of hematite at environmental oxygen pressures: Experimental surface phase diagram. Phys. Rev. B 75, 233406–233409. https://doi.org/10.1103/PhysRevB.75.233406

Burke, K., Wagner, L.O., 2013. DFT in a nutshell. Int. J. Quantum Chem. 113, 96–101. https://doi.org/10.1002/qua.24259

Campbell, C.T., Sellers, J.R.V., 2012. The entropies of adsorbed molecules. J. Am. Chem. Soc. 134, 18109–18115. https://doi.org/10.1021/ja3080117

Chinnam, N., Dey, S., Tripathi, S.N., Sharma, M., 2006. Dust events in Kanpur, northern India: Chemical evidence for source and implications to radiative forcing. Geophys. Res. Lett. 33, L08803–L08806. https://doi.org/10.1029/2005GL025278

Dreizler, R.M., Gross, E.K.U., 1990. Density functional theory: An approach to the quantum many-body problem, 1st ed. Springer-Verlag Berlin Heidelberg, Germany. https://doi.org/10.1007/978-3-642-86105-5

Engel, E., Dreizler, R.M., 2011. Density functional theory: An advanced course, 1st ed. Springer-Verlag Berlin Heidelberg, Germany. https://doi.org/10.1007/978-3-642-14090-7

Fry, A., Cauch, B., Silcox, G.D., Lighty, J.S., Senior, C.L., 2007. Experimental evaluation of the effects of quench rate and quartz surface area on homogeneous mercury oxidation. Proc. Combust. Inst. 31, 2855–2861. https://doi.org/10.1016/j.proci.2006.07.199

Gautier, S., Steinmann, S.N., Michel, C., Fleurat-Lessard, P., Sautet, P., 2015. Molecular adsorption at Pt(111). How accurate are DFT functionals? Phys. Chem. Chem. Phys. 17, 28921–28930. https://doi.org/10.1039/c5cp04534g

Gong, S.L., Barrie, L.A., Prospero, J.M., Savoie, D.L., Ayers, G.P., Blanchet, J.-P., Spacek, L., 1997. Modeling sea-salt aerosols in the atmosphere: 2. Atmospheric concentrations and fluxes. J. Geophys. Res. 102, 3819–3830. https://doi.org/10.1029/96JD03401

Hellman, A., Pala, R.G.S., 2011. First-principles study of photoinduced water-splitting on Fe_2O_3. J. Phys. Chem. C 115, 12901–12907. https://doi.org/10.1021/jp200751j

Jain, A., Seyed-Reihani, S.-A., Fischer, C.C., Couling, D.J., Ceder, G., Green, W.H., 2010. Ab initio screening of metal sorbents for elemental mercury capture in syngas streams. Chem. Eng. Sci. 65, 3025–3033. https://doi.org/10.1016/j.ces.2010.01.024

Jew, A.D., Rupp, E.C., Geatches, D.L., Jung, J.-E., Farfan, G., Bahet, L., Hower, J.C., Brown Jr., G.E., Wilcox, J., 2015. Mercury interaction with the fine fraction of coal-combustion fly ash in a simulated coal power plant flue gas stream. Energy Fuels 29, 6025–6038. https://doi.org/10.1021/acs.energyfuels.5b01253

Jung, J.-E., Geatches, D., Lee, K., Aboud, S., Brown Jr., G.E., Wilcox, J., 2015. First-principles investigation of mercury adsorption on the α-$Fe_2O_3(1\bar{1}02)$ surface. J. Phys. Chem. C 119, 26512–26518. https://doi.org/10.1021/acs.jpcc.5b07827

Koch, W., Holthausen, M.C., 2001. A chemist's guide to density functional theory, 2nd ed. Wiley-VCH, Germany. https://doi.org/10.1002/3527600043

Kresse, G., Furthmüller, J., 1996a. Efficiency of ab-initio total energy calculations for metals and semiconductors using a plane-wave basis set. Comput. Mater. Sci. 6, 15–50. https://doi.org/10.1016/0927-0256(96)00008-0

Kresse, G., Furthmüller, J., 1996b. Efficient iterative schemes for ab initio total-energy calculations using a plane-wave basis set. Phys. Rev. B 54, 11169–11186. https://doi.org/10.1103/PhysRevB.54.11169

Liu, Y., Göeltl, F., Ro, I., Ball, M.R., Sener, C., Aragão, I.B., Zanchet, D., Huber, G.W., Mavrikakis, M., Dumesic, J.A., 2017. Synthesis gas conversion over Rh-based catalysts promoted by Fe and Mn. ACS Catal. 7, 4550–4563. https://doi.org/10.1021/acscatal.7b01381

Lyman, S., Jones, C., O'Neil, T., Allen, T., Miller, M., Gustin, M.S., Pierce, A.M., Luke, W., Ren, X., Kelley, P., 2016. Automated calibration of atmospheric oxidized mercury measurements. Environ. Sci. Technol. 50, 12921–12927. https://doi.org/10.1021/acs.est.6b04211

Mishra, S.K., Dey, S., Tripathi, S.N., 2008. Implications of particle composition and shape to dust radiative effect: A case study from the Great Indian Desert. Geophys. Res. Lett. 35, L23814–L23818. https://doi.org/10.1029/2008GL036058

Mori, I., Nishikawa, M., Tanimura, T., Quan, H., 2003. Change in size distribution and chemical composition of kosa (Asian dust) aerosol during long-range transport. Atmos. Environ. 37, 4253–4263. https://doi.org/10.1016/S1352-2310(03)00535-1

Negreira, A.S., Aboud, S., Wilcox, J., 2011. Surface reactivity of V_2O_5(001): Effects of vacancies, protonation, hydroxylation, and chlorination. Phys. Rev. B 83, 045423–045436. https://doi.org/10.1103/PhysRevB.83.045423

Niksa, S., Fujiwara, N., 2005. Predicting extents of mercury oxidation in coal-derived flue gases. J. Air Waste Manage. Assoc. 55, 930–939. https://doi.org/10.1080/10473289.2005.10464688

Nørskov, J.K., Rossmeisl, J., Logadottir, A., Lindqvist, L., Kitchin, J.R., Bligaard, T., Jónsson, H., 2004. Origin of the overpotential for oxygen reduction at a fuel-cell cathode. J. Phys. Chem. B 108, 17886–17892. https://doi.org/10.1021/jp047349j

Parr, R.G., Yang, W., 1984. Density-functional theory of atoms and molecules, 1st ed. Oxford University Press, United Kingdom.

Rutter, A.P., Hanford, K.L., Zwers, J.T., Perillo-Nicholas, A.L., Schauer, J.J., Olson, M.L., 2008a. Evaluation of an offline method for the analysis of atmospheric reactive gaseous mercury and particulate mercury. J. Air Waste Manag. Assoc. 58, 377–383. https://doi.org/10.3155/1047-3289.58.3.377

Rutter, A.P., Schauer, J.J., 2007a. The effect of temperature on the gas-particle partitioning of reactive mercury in atmospheric aerosols. Atmos. Environ. 41, 8647–8657. https://doi.org/10.1016/j.atmosenv.2007.07.024

Rutter, A.P., Schauer, J.J., 2007b. The impact of aerosol composition on the particle to gas partitioning of reactive mercury. Environ. Sci. Technol. 41, 3934–3939. https://doi.org/10.1021/es062439i

Rutter, A.P., Schauer, J.J., Lough, G.C., Snyder, D.C., Kolb, C.J., Von Klooster, S., Rudolf, T., Manolopoulos, H., Olson, M.L., 2008b. A comparison of speciated atmospheric mercury at an urban center and an upwind rural location. J. Environ. Monit. 10, 102–108. https://doi.org/10.1039/b710247j

Sholl, D.S., Steckel, J.A., 2009. Density functional theory: A practical introduction, 1st ed. John Wiley and Sons, Inc., Hoboken, NJ. https://doi.org/10.1002/anie.200905551

Sliger, R.N., Kramlich, J.C., Marinov, N.M., 2000. Towards the development of a chemical kinetic model for the homogeneous oxidation of mercury by chlorine species. Fuel Process. Technol. 65–66, 423–438. https://doi.org/10.1016/S0378-3820(99)00108-3

Tacey, S.A., Xu, L., Mavrikakis, M., Schauer, J.J., 2016. Heterogeneous reduction pathways for Hg(II) species on dry aerosols: A first-principles computational study. J. Phys. Chem. A 120, 2106–2113. https://doi.org/10.1021/acs.jpca.5b12769

Tong, Y., Eichhorst, T., Olson, M.R., McGinnis, J.E., Turner, I., Rutter, A.P., Shafer, M.M., Wang, X., Schauer, J.J., 2013. Atmospheric photolytic reduction of Hg(II) in dry aerosols. Environ. Sci. Process. Impacts 15, 1883–1888. https://doi.org/10.1039/c3em00249g

Tong, Y., Eichhorst, T., Olson, M.R., Rutter, A.P., Shafer, M.M., Wang, X., Schauer, J.J., 2014. Comparison of heterogeneous photolytic reduction of Hg(II) in the coal fly ashes and synthetic aerosols. Atmos. Res. 138, 324–329. https://doi.org/10.1016/j.atmosres.2013.11.015

Wilcox, J., 2009. A kinetic investigation of high-temperature mercury oxidation by chlorine. J. Phys. Chem. A 113, 6633–6639. https://doi.org/10.1021/jp901050d

Wilcox, J., Rupp, E., Ying, S.C., Lim, D.-H., Negreira, A.S., Kirchofer, A., Feng, F., Lee, K., 2012. Mercury adsorption and oxidation in coal combustion and gasification processes. Int. J. Coal Geol. 90–91, 4–20. https://doi.org/10.1016/j.coal.2011.12.003

Xu, L., Stangland, E.E., Mavrikakis, M., 2018. A DFT study of chlorine coverage over late transition metals and its implication on 1,2-dichloroethane hydrodechlorination. Catal. Sci. Technol. 8, 1555–1563. https://doi.org/10.1039/c7cy02647a

Xu, L., Yao, X., Khan, A., Mavrikakis, M., 2016. Chloroform hydrodechlorination over palladium-gold catalysts: A first-principles DFT study. ChemCatChem 8, 1739–1746. https://doi.org/10.1002/cctc.201600144

Abstract Art

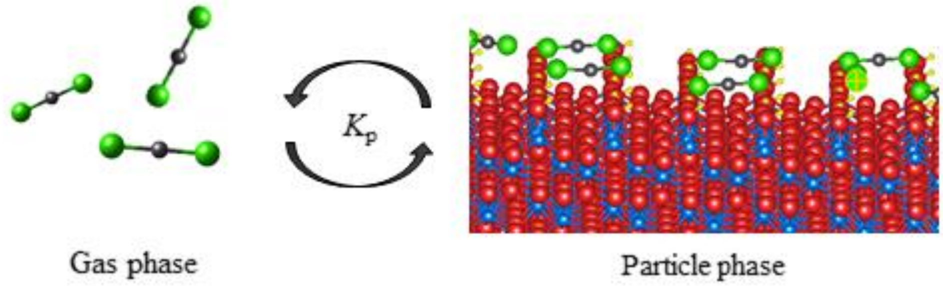
K_p
Gas phase
Particle phase